

# Variational approximations for traveling solitons in a discrete nonlinear Schrödinger equation

M Syafwan<sup>1,2</sup>, H Susanto<sup>1</sup>, S M Cox<sup>1</sup> and B A Malomed<sup>3</sup>

<sup>1</sup> School of Mathematical Sciences, University of Nottingham, University Park, Nottingham NG7 2RD, UK

<sup>2</sup> Department of Mathematics, Faculty of Mathematics and Natural Sciences, Andalas University, Limau Manis, Padang 25163, Indonesia

<sup>3</sup> Department of Physical Electronics, School of Electrical Engineering, Tel Aviv University, Tel Aviv 69978, Israel

E-mail: [hadi.susanto@nottingham.ac.uk](mailto:hadi.susanto@nottingham.ac.uk)

Received 23 August 2011, in final form 6 January 2012

Published 3 February 2012

Online at [stacks.iop.org/JPhysA/45/075207](http://stacks.iop.org/JPhysA/45/075207)

## Abstract

Traveling solitary waves in the one-dimensional discrete nonlinear Schrödinger equation with saturable onsite nonlinearity are studied. A variational approximation (VA) for the solitary waves is derived in analytical form. The stability is also studied by means of the VA, demonstrating that the solitons are stable, which is consistent with previously published results. Then, the VA is applied to predict parameters of traveling solitons with non-oscillatory tails (*embedded solitons*, ESs). Two-soliton bound states are considered too. The separation distance between the solitons forming the bound state is derived by means of the VA. A numerical scheme based on the discretization of the equation in the moving coordinate frame is derived and implemented using the Newton–Raphson method. In general, good agreement between the analytical and numerical results is obtained. In particular, we demonstrate the relevance of the analytical prediction of characteristics of the embedded solitons.

PACS numbers: 42.65.Tg, 05.45.Yv, 63.20.Pw

(Some figures may appear in colour only in the online journal)

## 1. Introduction

One of the major issues in studies of spatially discrete systems is whether such systems can support solitary waves that travel without losing energy to radiation, which results in deceleration and eventually pinning of the solitons. The celebrated Peierls–Nabarro (PN) barrier [1] is the reason that discrete systems do not generically support exponentially localized traveling solitary waves. The barrier corresponds to the energy difference between solutions for the onsite- and the intersite-centered lattice solitons, with the latter usually having a higher energy.

In the class of discrete systems, a ubiquitous model with profoundly important applications in physics and applied mathematics is the discrete nonlinear Schrödinger equation (DNLSE) [2]. One- and two-dimensional (1D and 2D) equations of this type are fundamental models of discrete nonlinear optics, representing planar and bulk arrays of nonlinear waveguides coupled by the tunneling of light between adjacent guiding cores [3]. Another well-known application of the DNLSE in any dimension is the description of Bose–Einstein condensates trapped in deep optical-lattice potentials, which split the condensate into an array of droplets [4].

The first attempt at finding traveling lattice solitons in the DNLSE was undertaken in [5], followed by a more systematic study in [6, 7]. The latter works indicate that traveling lattice solitons in the DNLSE are accompanied by nonzero radiation tails, which was confirmed by more recent studies [8, 9, 10].

While the most typical onsite nonlinearity in DNLSE models is cubic, waveguiding arrays made up of photorefractive materials feature the saturable nonlinearity, which strongly facilitates the creation of diverse discrete solitons [11], including solitary vortices [12], necklace-shaped sets [13], circular solitons [14] and symmetry-breaking modes [15]. Various higher order soliton patterns in the form of stable multi-charged vortices and ‘supervortices’ [16] have also been predicted in the framework of the same setting. Under appropriate conditions, the saturable nonlinearity may be approximated by a cubic–quintic truncation; 1D and 2D solitons in the DNLSE with the cubic–quintic onsite nonlinearity have also been studied in some detail [17]. It was thus found that the saturable nonlinearity readily supports traveling solitons in discrete media [18, 19]. A reason for this property is the fact that the PN barrier can change its sign in the case of the saturable nonlinearity [19]; hence, the barrier may vanish at isolated points. This property may be essential in finding lattice solitary waves that can travel permanently without emitting radiation (lattice phonons).

The saturable DNLSE modeling the propagation of optical waves in a photorefractive medium is

$$i \frac{du_n}{dt} = -\varepsilon \Delta_2 u_n(t) - \Lambda u_n(t) + \frac{\sigma u_n(t)}{1 + |u_n(t)|^2}, \quad (1)$$

where  $u_n$  is a complex-valued wavefunction at site  $n$ ,  $\varepsilon$  is the strength of the coupling between adjacent sites,  $\Delta_2 u_n(t) = u_{n+1}(t) - 2u_n(t) + u_{n-1}(t)$  is the 1D discrete Laplacian,  $-\Lambda$  is a background frequency and  $\sigma$  is the nonlinearity coefficient, which we scale to be  $\sigma = +1$ , implying that the onsite nonlinearity is self-focusing. Exact standing wave solutions of [1] have been derived in [20, 21]. To study traveling-wave solutions of equation (1), an ansatz of the form

$$u_n(t) = \psi(z, \tau) e^{ikn}, \quad (2)$$

with  $z \equiv n - ct$  and  $\tau \equiv t$ , is substituted to yield the time-dependent advance–delay-differential equation

$$i\psi_\tau(z, \tau) = ic\psi_z(z, \tau) + (2\varepsilon - \Lambda)\psi(z, \tau) - \varepsilon[\psi(z + 1, \tau) e^{ik} + \psi(z - 1, \tau) e^{-ik}] + \frac{\psi(z, \tau)}{1 + |\psi(z, \tau)|^2}, \quad (3)$$

where  $c$  and  $k$  are, respectively, the velocity and the wavenumber.

Traveling-wave solutions of equation (1) can be sought using the time-independent version of equation (3),

$$ic\psi' + (2\varepsilon - \Lambda)\psi(z) - \varepsilon[\psi(z + 1) e^{ik} + \psi(z - 1) e^{-ik}] + \frac{\psi(z)}{1 + |\psi(z)|^2} = 0, \quad (4)$$

with  $\psi' \equiv \frac{d\psi}{dz}$ . Equation (4) takes a simpler form in the case of  $k = 0$ , following [22, 23]:

$$ic\psi' + (2\varepsilon - \Lambda)\psi(z) - \varepsilon[\psi(z + 1) + \psi(z - 1)] + \frac{\psi(z)}{1 + |\psi(z)|^2} = 0. \quad (5)$$

The existence of traveling solitons for the DNLSSE of this type was investigated numerically by Melvin *et al* [22, 23], using a pseudo-spectral method to numerically solve equation (5), which yielded weakly delocalized solitary waves. The delocalization means that the traveling solitary waves in the saturable DNLSSE are, in general, accompanied by a nonzero oscillating tail, as frequency  $\Lambda$  will always resonate with the system's linear spectral (phonon) band. Because of this, a genuinely traveling solitary wave should be an *embedded soliton* (ES), which may exist inside the continuous spectrum, as an exceptional solution. (Note that the concept of ESs, which was originally developed for quiescent solitons in continuous media [24], was later extended to moving pulses [25] and to solitons in dynamical lattices [26].) Genuinely localized pulse-like solutions were then generated by finding zeros of the amplitude of the soliton's tail (the 'tail condition', which is similar to that used to single out ESs in the continuous family of delocalized intra-band quasi-solitons [24]). The stability of the numerically obtained solutions can then be analyzed in a numerical form by calculating the Floquet multipliers of the solutions, using methods similar to that developed in [8].

The presence of genuinely traveling lattice solitons in the saturable DNLSSE in the strong-coupling case has been shown analytically by Oxtoby and Barashenkov, using exponential asymptotic methods [27] (see also [10]). The use of this sophisticated technique is necessary, as the radiation emitted by moving solitary waves is exponentially small in the wave's amplitude. This is a reason why broad, small-amplitude pulses are highly mobile, seeming like freely traveling solitons.

In this paper we apply, for the first time, a variational approximation (VA) to the study of traveling solitary waves and their stability, as well as for predicting the location of the genuinely localized traveling solitary waves. In the context of DNLSSE with cubic nonlinearity, the application of VA was proposed to construct the fundamental onsite and intersite soliton solutions by using a trial function containing unknown parameters that have to be found using the Euler–Lagrange equations [28, 29]. The same VA method has been applied recently to the cubic–quintic DNLSSE [30] (see also [31] and references therein). It was shown that the method is not only excellent in approximating the fundamental discrete solitons, but also correctly predicts their stability.

The rest of the paper is organized as follows. In section 2, we develop the VA for the solitary-wave solutions of the advance–delay equation. In the same section, we derive an analytical function whose zeros correspond to the location of ESs. The use of the VA in analyzing the stability of the traveling solitary waves is then discussed. In addition to single-hump pulses, in the same section we consider bound states built from two solitons, and the use of the VA to predict the distance between them. In section 3, we introduce a numerical scheme for solving equation (5) and compare the numerical results with the analytical calculations performed in the preceding section. Results of the work are summarized in section 4.

## 2. The variational approximation

### 2.1. Core soliton solutions

As suggested by the previous work [8], a traveling lattice wave may be considered as a superposition of an exponentially localized *core* and extended background built of finite-amplitude plane waves. Here, we first derive the VA for the core. To this end, we recall that equation (5) can be represented in the variational form

$$\delta L / \delta \psi^*(z) = 0, \quad (6)$$

where  $\delta/\delta\psi^*$  stands for the variational derivative of a functional, the asterisk denotes complex conjugation and the Lagrangian is

$$L = \int_{-\infty}^{+\infty} \left[ (2\varepsilon - \Lambda)|\psi|^2 + \ln(1 + |\psi|^2) + \frac{ic}{2}[\psi^*\psi' - \psi(\psi')^*] - \frac{\varepsilon}{2}\{\psi^*[\psi(z+1) + \psi(z-1)] + \psi[\psi^*(z+1) + \psi^*(z-1)]\} \right] dz. \quad (7)$$

A suitable trial function, or *ansatz*, may be chosen as

$$\psi_{\text{core}}(z) = F(z) \exp(ipz), \quad (8)$$

$$F(z) = A \operatorname{sech}(az), \quad (9)$$

where  $A$ ,  $a$  and  $p$  are the real variational parameters. While this *ansatz* postulates exponential tails of the soliton, the prediction of solitons within the framework of the VA does not necessarily mean that the corresponding solitons exist in a rigorous sense, as the actual tail may be non-vanishing at  $|z| \rightarrow \infty$ . In fact, the prediction of solitons by the VA may imply a situation in which the amplitude of the non-vanishing tail is not zero, but attains its minimum [32].

The next step is to substitute *ansatz* (8) into Lagrangian (7), perform the integration and derive the Euler–Lagrange equations

$$\partial L/\partial A = \partial L/\partial a = \partial L/\partial p = 0. \quad (10)$$

By substituting *ansatz* (8) into the Lagrangian and performing the integration, we obtain the following effective Lagrangian, as a function of parameters  $A$ ,  $a$  and  $p$ :

$$L_{\text{eff}} = \frac{2A^2(2\varepsilon - \Lambda - cp)}{a} + \frac{\ln^2(\sqrt{1+A^2}+A) + \ln^2(\sqrt{1+A^2}-A)}{a} - \frac{4A^2\varepsilon \cos(p)}{\sinh(a)}. \quad (11)$$

Then, substituting Lagrangian (11) into equations (10) yields the following equations:

$$\frac{A(2\varepsilon - \Lambda - cp)}{a} + \frac{\ln(\sqrt{1+A^2}+A)}{a\sqrt{1+A^2}} - \frac{2A\varepsilon \cos(p)}{\sinh(a)} = 0, \quad (12)$$

$$-\frac{2A^2(2\varepsilon - \Lambda - cp)}{a^2} - \frac{\ln^2(\sqrt{1+A^2}+A) + \ln^2(\sqrt{1+A^2}-A)}{a^2} + \frac{4A^2\varepsilon \cos(p) \cosh(a)}{\sinh^2(a)} = 0, \quad (13)$$

$$-\frac{c}{a} + \frac{2\varepsilon \sin(p)}{\sinh(a)} = 0. \quad (14)$$

This system of algebraic equations for  $A$ ,  $a$  and  $p$  can be solved numerically.

## 2.2. Prediction of the VA for embedded solitons

We now seek a condition for the possible existence of ESs. To do so, we begin by considering a delocalized solution of the linearized version of equation (5),  $\psi_{\text{bckg}}(z)$ , which represents the non-vanishing background. Then, following [32], it can be shown that the condition for the possible existence of ESs, i.e. the absence of nonzero backgrounds attached to the soliton, is the natural orthogonality relation

$$\int_{-\infty}^{+\infty} \{ \delta L/\delta\psi^* |_{\psi(z)=\psi_{\text{core}}(z)} \psi_{\text{bckg}}^*(z) + \text{c.c.} \} dz = 0, \quad (15)$$

where c.c. stands for the complex conjugate of the preceding expression and the variational derivative  $\delta L/\delta\psi^*|_{\psi(z)=\psi_{\text{core}}(z)}$  is the left-hand side of equation (5) with  $\psi(z)$  replaced by  $\psi_{\text{core}}(z)$ . In the context of the VA,  $\psi_{\text{core}}(z)$  in equation (15) should be substituted by the (approximate) form corresponding to the soliton. Here, the background function is taken as

$$\psi_{\text{bckg}}(z) = \psi_0 \exp(i\lambda z), \quad (16)$$

with a constant amplitude  $\psi_0$ , while the soliton's core is approximated by ansatz (8). Next, the frequency  $\lambda$  of the oscillating background in equation (16) can be found by substituting  $\psi_{\text{bckg}}$  into the linearization of equation (5), i.e.

$$i c \frac{d\psi}{dz} + (2\varepsilon - \Lambda + 1) \psi(z) - \varepsilon [\psi(z+1) + \psi(z-1)] = 0, \quad (17)$$

which yields

$$c\lambda + (\Lambda - 1) - 2\varepsilon (1 - \cos(\lambda)) = 0. \quad (18)$$

By setting  $\psi_0 = \alpha + i\beta$ , where  $\alpha$  and  $\beta$  are nonzero real constants, equation (15) yields

$$\int_{-\infty}^{+\infty} (\alpha \mathcal{M} + \beta \mathcal{N}) dz = 0, \quad (19)$$

where we define functions

$$\begin{aligned} \mathcal{M}(z) = & \left\{ (2\varepsilon - c\lambda - \Lambda) F(z) + \frac{F(z)}{1 + F(z)^2} \right\} \cos((\lambda - p)z) \\ & - \varepsilon [F(z+1) \cos((\lambda - p)z - p) + F(z-1) \cos((\lambda - p)z + p)], \end{aligned} \quad (20)$$

$$\begin{aligned} \mathcal{N}(z) = & \left\{ (2\varepsilon - c\lambda - \Lambda) F(z) + \frac{F(z)}{1 + F(z)^2} \right\} \sin((p - \lambda)z) \\ & - \varepsilon [F(z+1) \sin((p - \lambda)z + p) + F(z-1) \sin((p - \lambda)z - p)]. \end{aligned} \quad (21)$$

It is readily checked that  $\mathcal{N}(z)$  is an odd function, while  $\mathcal{M}(z)$  is an even one. Therefore, after some manipulations, integral relation (19) may be cast into the form

$$\int_0^{+\infty} \left[ \frac{(2\varepsilon - c\lambda - \Lambda) \cos((\lambda - p)z)}{\cosh(az)} - \frac{2 \cosh(az) \cos((\lambda - p)z)}{\cosh(2az) + 1 + 2A^2} - \frac{\mathcal{B}\varepsilon \cos((\lambda - p)z) \cosh(az)}{\cosh(2az) + \cosh(2a)} + \frac{\mathcal{C}\varepsilon \sin((\lambda - p)z) \sinh(az)}{\cosh(2az) + \cosh(2a)} \right] dz = 0, \quad (22)$$

with  $\mathcal{B} \equiv 4 \cos(p) \cosh(a)$  and  $\mathcal{C} \equiv 4 \sin(p) \sinh(a)$ . The integrals in the first and the last terms are evaluated using formulas (3.981–3) and (3.983–5), while the second and the third terms are evaluated using (3.984–4), from tables of integrals given in [33]. The calculation yields

$$E \equiv (2\varepsilon - c\lambda - \Lambda) - 2\varepsilon \cos(\lambda) + \frac{\cos([\lambda - p] \cosh^{-1}(1 + 2A^2)]/2a}{\cosh([\cosh^{-1}(1 + 2A^2)]/2)} = 0, \quad (23)$$

provided that  $a > 0$  and  $\lambda > p$ . Thus, in the framework of the VA, equation (23), along with the results of the VA for the soliton's core given by equations (12)–(14), and with equation (18), may predict a curve—in particular, in the  $(\lambda, \varepsilon)$  plane—along which the existence of the ESs may be expected.

### 2.3. The VA-based stability analysis

Here, we propose to use the VA to study the stability of the core of the traveling lattice solitary wave by calculating eigenvalues for modes of small perturbations in the moving coordinate frame, following [34]. The stability of the background, i.e. the modulational (in)stability of the plane lattice waves, was studied in [8].

The underlying time-dependent equation (3) with  $k = 0$  simplifies to

$$-ic\psi_z(z, \tau) + i\psi_\tau(z, \tau) = (2\varepsilon - \Lambda)\psi(z, \tau) - \varepsilon[\psi(z + 1, \tau) + \psi(z - 1, \tau)] + \frac{\psi(z, \tau)}{1 + |\psi(z, \tau)|^2}. \quad (24)$$

The Lagrangian of equation (24) is

$$L = \int_{-\infty}^{+\infty} \left[ (2\varepsilon - \Lambda)|\psi|^2 + \ln(1 + |\psi|^2) + \frac{ic}{2}[\psi^*\psi_z - \psi\psi_z^*] - \frac{\varepsilon}{2}\{\psi^*[\psi(z + 1, \tau) + \psi(z - 1, \tau)] + \psi[\psi^*(z + 1, \tau) + \psi^*(z - 1, \tau)]\} - \frac{i}{2}(\psi^*\psi_\tau - \psi\psi_\tau^*) \right] dz. \quad (25)$$

Note that equation (24) is produced by the variation with respect to  $\psi^*$  not of Lagrangian (25), but rather of the corresponding action functional,  $S = \int L dt$ . However, for practical purposes (the derivation of VA equations), it is enough to calculate Lagrangian (25) (it is not necessary to calculate the action functional explicitly). The time-dependent ansatz, generalizing the static one (8), is

$$\psi_{\text{core}}(z, \tau) = A(\tau)\text{sech}[a(\tau)(z - \xi(\tau))] \times \exp\left(i\phi(\tau) + ip(\tau)z + \frac{i}{2}C(\tau)[z - \xi(\tau)]^2\right), \quad (26)$$

where all parameters are real functions of time. Additional variational parameters which appear here are the coordinate of soliton's center,  $\xi(\tau)$ , the overall phase,  $\phi(\tau)$ , and the intrinsic chirp,  $C(\tau)$ . Substituting ansatz (26) into Lagrangian (25) and performing the integration yields the corresponding effective Lagrangian,

$$L_{\text{eff}} = A(\tau)^2 \left\{ \frac{-2\Lambda + \varepsilon Q(\tau) + 2[\xi(\tau)p'(\tau) + \phi'(\tau) - cp(\tau)]}{a(\tau)} + \frac{\pi^2 C'(\tau)}{12a(\tau)^3} \right\} + \frac{\ln^2(\sqrt{1 + A(\tau)^2} + A(\tau)) + \ln^2(\sqrt{1 + A(\tau)^2} - A(\tau))}{a(\tau)}, \quad (27)$$

with primes standing for the derivatives and

$$Q(\tau) \equiv 4 - \frac{4\pi \sin\left(\frac{C(\tau)}{2}\right) \cos(p(\tau))}{\sinh(a(\tau)) \sinh\left(\frac{C(\tau)\pi}{2a(\tau)}\right)} = 4 - \frac{4a(\tau) \cos(p(\tau))}{\sinh(a(\tau))} + \frac{(a(\tau)^2 + \pi) \cos(p(\tau))C(\tau)^2}{6a(\tau) \sinh(a(\tau))} + \mathcal{O}(C^4). \quad (28)$$

The Euler–Lagrange equations for the variational parameters take the form of an ODE system, which may be symbolically written in the vectorial form,  $\mathbf{x} \equiv [A'(\tau), a'(\tau), p'(\tau), C'(\tau), \phi'(\tau), \xi'(\tau)]^T = \mathbf{g}(\mathbf{x})$ , and solved numerically. The VA-predicted stability analysis is based on the linearization

$$\mathbf{z} = \mathbf{x}_0 + \delta\mathbf{y}, \quad (29)$$

with infinitesimal  $\delta$ , and  $\mathbf{x}_0 = [A, a, p, C = 0, \phi = 0, \xi = 0]^T$  representing solutions of static variational equations (12)–(14). The substitution of this into the dynamical Euler–Lagrange equations and linearization leads to an eigenvalue problem

$$\dot{\mathbf{y}} = \mathbf{H}\mathbf{y}, \tag{30}$$

with the corresponding stability matrix  $\mathbf{H}$ . The stability of the stationary solution is then determined by the eigenvalues  $\Omega$  of equation (30), which must be found in numerical form, the solution being stable if  $\text{Re}(\Omega) \leq 0$  for all eigenvalues.

#### 2.4. The effective potential of the soliton–soliton interaction and the formation of bound states

DNLSEs are known to admit bound states of fundamental (single-humped) solitons [35–37]. The present model also supports bound states, in addition to the single-hump solitons. In the infinite domain, there are infinitely many different bound states. An essential feature of such states is that the distances between the bound solitons are not arbitrary. In the weak-interaction limit, this feature may be explained by means of the VA, as we indicate below.

The effective potential for the interaction between two *identical* solitons separated by distance  $|l|$ , which is essentially larger than the width of each soliton, and with a phase shift  $\phi$  between them ( $\phi \equiv \phi_2 - \phi_1$ , where  $\phi_{1,2}$  are the phases at central points of the two solitons), can be derived following the general approach elaborated in [38, 39]. To this end, we consider the wave field in the vicinity of one of the two solitons (say, soliton number 1), whose center is located at  $z = 0$ , while the other soliton (number 2) is located far afield, at  $z = l$ ; thus, we set

$$\psi(z) = \psi_1(z) + \psi_2(z). \tag{31}$$

Here,  $\psi_2$  is realized as a weak tail of the second soliton. (Of course, the tail is affected by the overlap with soliton number 1.) Then, expression (31) is substituted into the Hamiltonian ( $H$ ) corresponding to Lagrangian (7). The effective interaction potential is represented by the corresponding term in the total Hamiltonian, which is linearized in the weak field,  $\psi_2$ . Thus, the corresponding contribution to the potential is

$$U_{12} = \int_{-\infty}^{+\infty} \left[ \frac{\delta H}{\delta \psi(z)} \psi_2(z) + \frac{\delta H}{\delta \psi^*(z)} \psi_2^*(z) \right] dz, \tag{32}$$

where the variational derivatives are taken at  $\psi_2 = 0$  (i.e. for  $\psi = \psi_1$ , see equation (31)). The integral is formally written over an infinite domain, although it is assumed that it will be calculated in the vicinity of the first soliton (see below).

Because the stationary one-soliton solution is itself found from the equation

$$\frac{\delta H}{\delta \psi(z)} = 0, \tag{33}$$

with  $\psi = \psi_1$ , it might seem that expression (32) should identically vanish. (The variational derivatives corresponding to the single-soliton solution should be zero, according to equation (33).) However, the integral will in fact vanish only after performing the integration by parts of the terms which contain the first derivative of  $\psi_2$ :

$$\frac{ic}{2} \int_{-\infty}^{+\infty} \left[ \psi_1^* \frac{\partial \psi_2}{\partial z} - \psi_1 \left( \frac{\partial \psi_2}{\partial z} \right)^* \right] dz. \tag{34}$$

Thus, the sole nonzero contribution to  $U_{12}$  originates from the surface term produced by the integration by parts in expression (34):  $U_{12} = (ic/2) \Delta \{ \psi_1^* \psi_2 - \psi_1 \psi_2^* \}$ , where the notation  $\Delta \{ \dots \}$  denotes the difference between the values of this expression at two arbitrary points,  $Z_-$  and  $Z_+$ , located sufficiently far from the center of the first soliton (on its left and right sides,

respectively), but so that the second soliton remains much further still. In fact, one can take  $Z_- = -\infty$ , while  $Z_+$  is an arbitrary intermediate point between the two solitons, located far from both, but closer to the first soliton. Finally, the total interaction potential also includes a symmetric contribution from the vicinity of the second soliton:

$$U_{\text{int}} = U_{12} + U_{21} = \frac{1}{2}ic\Delta(\{\psi_1^*\psi_2 - \psi_1\psi_2^*\} + \{\psi_2^*\psi_1 - \psi_2\psi_1^*\}). \quad (35)$$

The main trick (which was employed in [38, 39]) is to use the asymptotic expressions for the wave fields of both solitons taken far from their respective centers (i.e. their *tails*). To this end, we first consider the *linearized* equation (17), with soliton tails sought in the form of

$$\psi(z) = \psi^{(0)} e^{\lambda_{\text{ap}}z}, \quad (36)$$

where constant  $\psi^{(0)}$  is determined by the full nonlinear solution. In fact, expression (36) can be viewed as a limiting form of ansatz (8) as  $|z| \rightarrow \infty$ , such that  $\psi^{(0)} = 2A$  and  $\lambda_{\text{ap}} = a + ip$ . Note the similarity between expressions (36) and (16), the only difference being that  $\lambda$  was real, whereas  $\lambda_{\text{ap}}$  may be complex. Replacing  $\lambda$  by  $-i\lambda_{\text{ap}}$  in (18), we find that  $\lambda_{\text{ap}}$  then satisfies equation

$$ic\lambda_{\text{ap}} + (2\varepsilon - \Lambda + 1) - 2\varepsilon \cosh(\lambda_{\text{ap}}) = 0. \quad (37)$$

It is evident that if  $\lambda_{\text{ap}}$  is a complex root of equation (37), then  $-\lambda_{\text{ap}}^*$  is also a root. Thus, the pair of complex roots may be defined through their real and imaginary parts as  $\pm\lambda_r + i\lambda_i$ , where  $\lambda_r$  is chosen to be positive, by definition. In this regard, the transcendental complex equation (37) may be cast into an explicit form if  $\lambda_r$  and  $\lambda_i$  are treated as free parameters, while  $c$  and  $\Lambda$  are considered as unknowns. This approach yields

$$c = \frac{2\varepsilon}{\lambda_r} \sinh(\lambda_r) \sin(\lambda_i), \quad (38)$$

$$\Lambda = 1 + 2\varepsilon \left[ 1 - \cosh(\lambda_r) \cos(\lambda_i) + \frac{\lambda_i}{\lambda_r} \sinh(\lambda_r) \sin(\lambda_i) \right]. \quad (39)$$

Then, equation (36) yields the tails of the two solitons in the form of

$$\psi_1(z) \approx \psi^{(0)} \exp(-\lambda_r|z| + i\lambda_i z), \quad (40)$$

$$\psi_2(z) \approx \psi^{(0)} \exp(-\lambda_r|z - l| + i\lambda_i(z - l)). \quad (41)$$

(Recall that the centers of solitons numbers 1 and 2 are assumed to be located at  $z = 0$  and  $z = l$ , respectively.) The substitution of expressions (40)–(41) into equation (35) yields an explicit result, which *does not* depend on arbitrary intermediate point  $Z_+$  appearing in the expression for  $U_{12}$  (nor does it depend on the counterpart of  $Z_+$  arising in  $U_{21}$ ) because contributions from  $Z_+$  *cancel out* in the final expression (cf [38, 39]). We thus obtain the following expression for the interaction potential (35):

$$U_{\text{int}}(l) = 2c|\psi^{(0)}|^2 \exp(-\lambda_r l) \sin(\lambda_i l - \phi), \quad (42)$$

where the above-mentioned phase shift is taken into account. In this expression, everything is known, in principle (recall that  $\psi^{(0)}$  is to be found from the full nonlinear solution for one soliton), if the phase shift  $\phi$  is considered as a given *frozen* constant.

Strictly speaking, the exponentially decaying potential (42) is valid for solitons whose waveforms are fully localized. If the actual shape of the solitons features small non-vanishing oscillating tails, the asymptotic form of the potential at large values of  $l$  will change accordingly.

It is straightforward to see that potential (42) gives rise to a set of local minima and maxima (as a function of  $l$ ), which may correspond to a series of two-soliton bound states, as

well as to more complex multi-soliton bound ones. The extrema of the potential are located at points

$$l_n = \frac{1}{\lambda_i} \arctan\left(\frac{\lambda_i}{\lambda_r}\right) + \frac{\phi + \pi n}{\lambda_i}, \quad n \cdot \text{sign}(\lambda_i) = 0, 1, 2, 3, \dots \quad (43)$$

The extrema are potential minima for even or odd integers (i.e. for  $n \cdot \text{sign}(\lambda_i) = 0, 2, 4, \dots$  or  $n \cdot \text{sign}(\lambda_i) = 1, 3, 5, \dots$ , severally), at  $c\lambda_i/\lambda_r < 0$  and  $c\lambda_i/\lambda_r > 0$ , respectively. Note that the separation between the potential minima,  $\Delta l = \pi/|\lambda_i|$ , does not depend on the frozen phase shift,  $\phi$ .

### 3. Numerical scheme and comparisons with analytical results

To solve equation (5) numerically, we use a scheme based on the discretization of the equation, resulting in a system of difference equations. We employ central finite differences, so that the corresponding Jacobian matrix is sparse. The difference equations are then solved using the Newton–Raphson method. This is different from the previously used pseudo-spectral collocation method [23], in which the dependent variable  $\psi$  was represented as a Fourier series, whose coefficients were then determined by solving a system of algebraic equations obtained by requiring the series approximation to satisfy the governing equation at collocation points.

In the framework of the finite-difference method, with grid size  $\Delta z$ , we approximate  $\psi(z)$  on a finite interval,  $[-L, +L]$ , as follows:  $\psi(z) \rightarrow \psi(n\Delta z) \equiv \psi_n$ ,  $\psi(z \pm 1) \rightarrow \psi((n \pm 1/\Delta z)\Delta z) = \psi_{n \pm 1/\Delta z}$ . For  $\psi'(z) \equiv \frac{d\psi}{dz}$ , we use either the central two-point stencil,  $(\psi_{n+1} - \psi_{n-1})/(2\Delta z)$ , or the spectral collocation method [40, 41]. In the following, we describe details of the numerical scheme for the two-point stencil, although the spectral collocation method has been implemented too.

Substituting the above discretizations into equation (5) yields

$$\frac{ic}{2\Delta z}(\psi_{n+1} - \psi_{n-1}) + (2\varepsilon - \Lambda)\psi_n - \varepsilon(\psi_{n+1/\Delta z} + \psi_{n-1/\Delta z}) + \frac{\psi_n}{1 + |\psi_n|^2} = 0. \quad (44)$$

The number of grid points is  $N = 2L/\Delta z + 1$ . We use periodic boundary conditions, so that  $\psi_{N-1+j} = \psi_j$  and  $\psi_{1-j} = \psi_{N-j}$  for  $j = 1, 2, \dots, M$ , where  $M \equiv 1/\Delta z$ .

Next, we solve the resulting system of nonlinear equations (44) numerically for a fixed set of parameters  $(c, \varepsilon, \Lambda)$ , using the Newton–Raphson method with an error tolerance of order  $10^{-15}$ . To do so, we define the left-hand side of equation (44) as  $f_n$  and then seek a solution with  $f_n = 0$  for  $n = 1, 2, \dots, N - 1$ . Because  $\psi$  is complex, we seek solutions in the form of  $\psi = \text{Re}(\psi) + i \text{Im}(\psi)$ . Accordingly, we define a (real) functional vector,  $\mathbf{F} \equiv [\text{Re}(f_1), \dots, \text{Re}(f_{N-1}), \text{Im}(f_1), \dots, \text{Im}(f_{N-1})]^T$ , and a (real) solution vector,  $\mathbf{\Psi} \equiv [\text{Re}(\psi_1), \dots, \text{Re}(\psi_{N-1}), \text{Im}(\psi_1), \dots, \text{Im}(\psi_{N-1})]^T$ . Note that equation (5) has rotational and translational invariance. Therefore, to ensure the uniqueness of the solutions, we impose two constraints,

$$\begin{aligned} f_{\frac{N+1}{2}+1} &= \text{Re}(\psi_{\frac{N+1}{2}-1}) - \text{Re}(\psi_{\frac{N+1}{2}+1}) = 0, \\ f_{\frac{N+1}{2}+N} &= \text{Im}(\psi_{\frac{N+1}{2}}) = 0. \end{aligned} \quad (45)$$

These constraints significantly improve the convergence of the Newton–Raphson scheme.

Strictly speaking, we do not have a rigorous proof of the convergence of the numerical scheme outlined above. Therefore, to check the validity of our findings, we benchmarked the results against those reported in [23] for the same parameter values. The outputs (not shown here) were indeed identical for  $\Delta z$  small enough and  $L$  large enough. Below, we display results for  $L = 50$  and  $\Delta z = 0.2$ , which is sufficient for clear presentation. We have also used smaller values of  $\Delta z$  and larger  $L$ , which confirmed the robustness of the results.

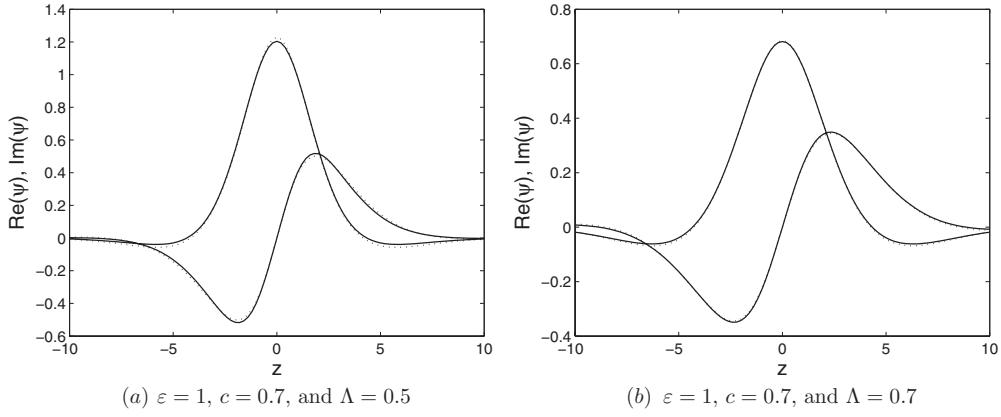


**Figure 1.** The comparison of two soliton profiles for two different values of  $\Lambda$ , as indicated in the caption to each panel. The solid lines correspond to numerical results, i.e. solutions of equation (44) imposed with constraints (45), with  $\Delta z = 0.2$  and  $L = 50$  (the  $z$ -axis is truncated to focus the picture on the soliton's core), both the real and imaginary parts being shown. The dotted lines are predictions of the variational approximation obtained through solving equations (12)–(14).

### 3.1. The soliton's core

For given parameters  $\varepsilon, c$  and  $\Lambda$ , we solve the variational equations (12)–(14) to produce suitable real solutions  $A, a$  and  $p$ , which then give a quasi-analytical approximation for the soliton's core described by the function  $\psi_{\text{core}}(z)$  (see equation (8)). As generic examples, in figure 1 we present, at  $\varepsilon = 1$  and  $c = 0.7$ , the comparison of two soliton profiles obtained from the numerical results and VA for two different values of  $\Lambda$ . We have found  $A \approx 1.228, a \approx 0.554, p \approx 0.377$  for  $\Lambda = 0.5$  (figure 1(a)), and  $A \approx 0.685, a \approx 0.414, p \approx 0.368$  for  $\Lambda = 0.7$  (figure 1(b)). Particularly good agreement is observed in both cases.

To further confirm the agreement for different values of  $\Lambda, \varepsilon$  and  $c$ , in the following we compare the parameters  $A, a$  and  $p$  produced by the VA with their numerical counterparts. To calculate the latter, we make use of the following relations, which are generated by ansatz (8), (9) at  $z = 0$ :

$$\psi(0) = A, \quad \psi'(0) = ipA, \quad \psi''(0) = -A(a^2 + p^2), \quad (46)$$

and take the left-hand sides of these relations from numerical data. Thus, using the central finite differences, we obtain the numerical counterparts of  $A, p$  and  $a$ :

$$A_{\text{num}} = \psi_{\frac{N+1}{2}}, \quad (47)$$

$$p_{\text{num}} = \frac{\text{Im}(\psi_{\frac{N+1}{2}+1}) - \text{Im}(\psi_{\frac{N+1}{2}-1})}{2A\Delta z}, \quad (48)$$

$$a_{\text{num}} = \pm \sqrt{-\frac{\text{Re}(\psi_{\frac{N+1}{2}-1}) - 2\text{Re}(\psi_{\frac{N+1}{2}}) + \text{Re}(\psi_{\frac{N+1}{2}+1})}{A_{\text{num}}(\Delta z)^2} - p_{\text{num}}^2}. \quad (49)$$

The comparison of the parameters  $A, a$  and  $p$  obtained numerically (solid line) and from the VA (dashed line) is shown in figure 2(a) for varying  $1/\varepsilon$  and fixed  $(c, \Lambda) = (0.7, 0.5)$ . We observe that the solid and dashed curves are generally close for all three parameters.

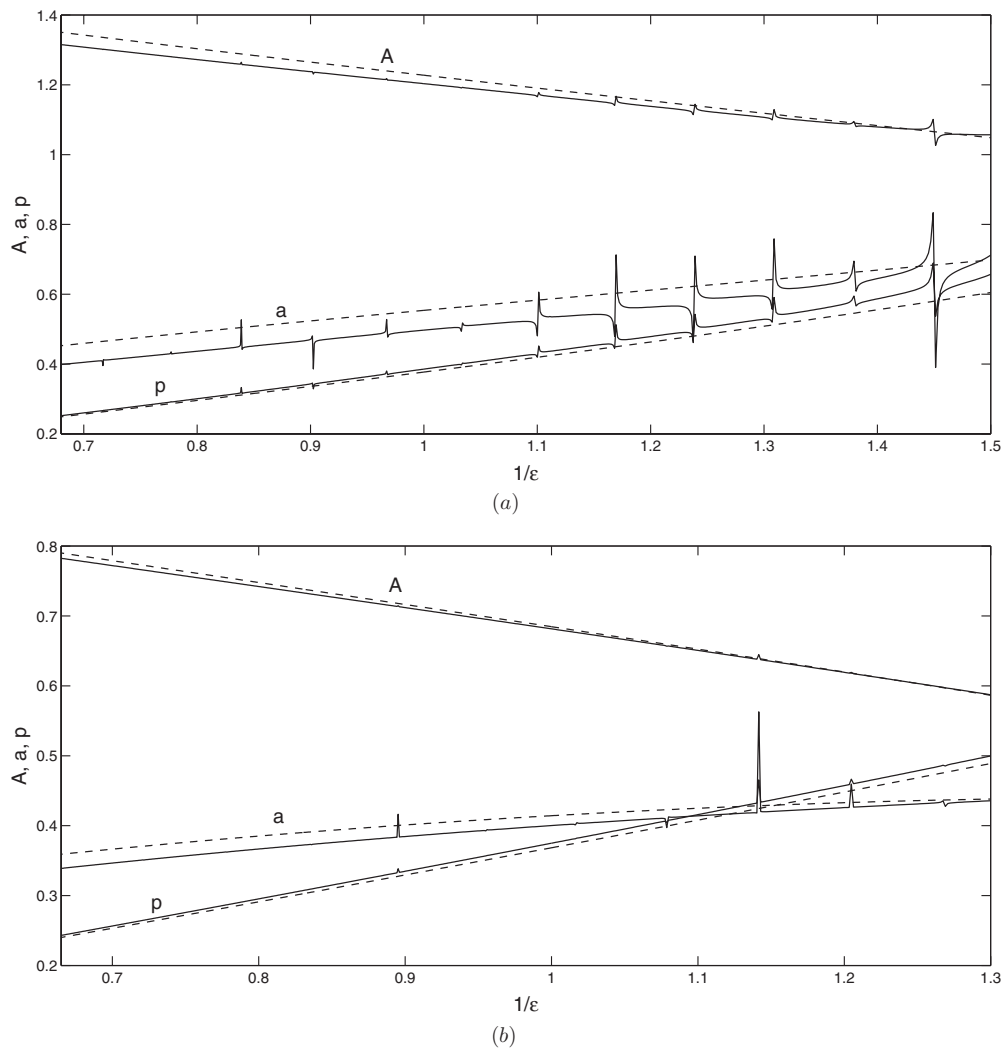


**Figure 2.** The comparison of parameters  $A$ ,  $a$  and  $p$  calculated from the numerical data (solid lines) through equations (47)–(49), and from the VA (dashed lines) through equations (46), for  $c = 0.7$  and  $\Lambda = 0.5$  (a) or  $\Lambda = 0.7$  (b) for varying  $1/\epsilon$ .

Nevertheless, we also find isolated values of  $1/\epsilon$ , which behave as singular points. Near the singularities the numerical results deviate very rapidly from the predictions of the VA. In fact, at these singular points the numerically obtained solutions are strongly delocalized due to the resonance of the oscillating tails with the finite size of the computational domains, hence, the positions of such singularities depend on  $L$ , and they may be considered as artifacts of approximating the infinite region by the finite domain.

Similar to figure 1, where a better approximation is obtained for larger  $\Lambda$ , we also observe in figure 2(b) that the variational and numerical curves for  $A$ ,  $a$  and  $p$  are closer for  $\Lambda = 0.7$  than those in figure 2(a). In the latter case, the singularities are present too, even though they are less pronounced here.

Thus, we can conclude that the VA provides a reliable approximation for the description of the soliton’s core.

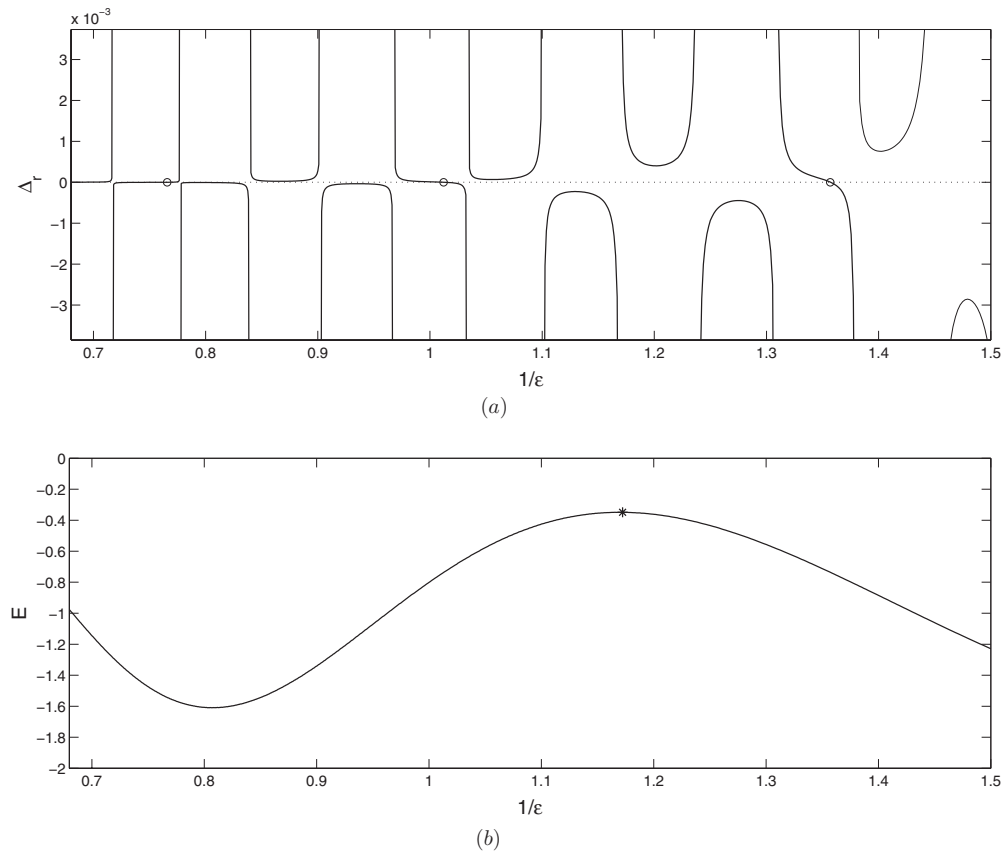


**Figure 3.** (a) The signed measure  $\Delta_r$  (cf equation (51)) as a function of  $1/\varepsilon$  for  $c = 0.7$ ,  $\Lambda = 0.5$ ,  $\Delta z = 0.2$  and  $L = 50$ , where  $\Delta_r$  is zero at  $\varepsilon \approx 0.737, 0.988, 1.306$  (or at  $1/\varepsilon \approx 1.357, 1.012, 0.766$ ), as shown by empty circles. (b)  $E$  versus  $1/\varepsilon$  (cf equation (23)), for the same parameter values ( $\Lambda, c$ ) as in panel (a) and for the corresponding solutions for  $(A, a, p)$  and root(s)  $\lambda$  obtained from equations (12)–(14) and (18), respectively. It is clearly seen that  $E \neq 0$  in the observed domain of  $1/\varepsilon$ . However, we can conjecture that ESs are located near the maximum of  $E$ , i.e. at  $\varepsilon \approx 0.853$  (or at  $1/\varepsilon \approx 1.172$ ), as indicated by the star.

### 3.2. Embedded solitons

As shown in [23], in the general case the numerically obtained solitary waves are weakly delocalized, i.e. oscillatory tails with a non-vanishing amplitude are attached to them. Nevertheless, as suggested in [22, 23], it is possible to find solutions with vanishing tails (i.e. genuine solitons) by considering quantity

$$\Delta_i = \text{Im}(\psi(N)), \tag{50}$$

which is a signed measure, whose zeros correspond to solutions with vanishing tails. In the present case, the periodic boundary conditions lead to  $\text{Im}(\psi(N)) = 0$ , since the imaginary part of  $\psi$  is odd. Therefore, we modify the signed measure (50) and redefine it as

$$\Delta_r = \text{Re}(\psi(N)). \tag{51}$$

In figure 3(a),  $\Delta_r$  is plotted as a function of  $1/\varepsilon$  for the parameter values ( $\Lambda, c, \Delta z, L$ ) used in figure 2(a). We see from the figure that zeros of  $\Delta_r$  occur at  $\varepsilon \approx 0.737, 0.988, 1.306$

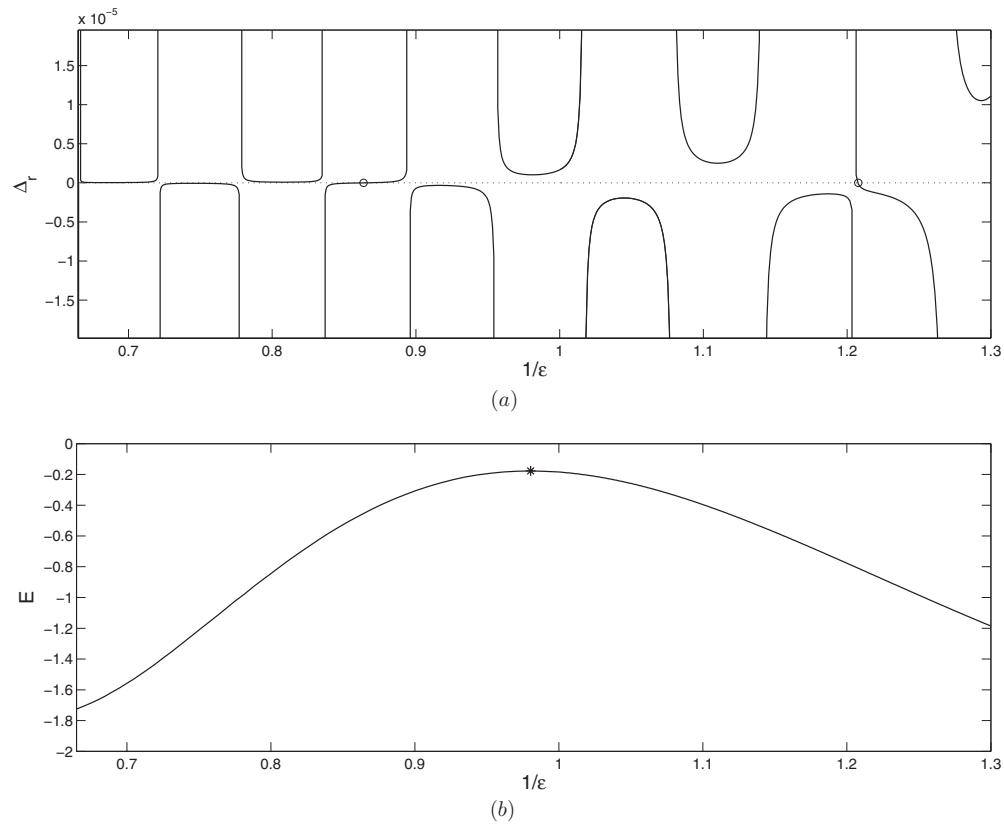


**Figure 4.** The same as figure 3, but for  $\Lambda = 0.7$ . Zeros of  $\Delta_r$  are found at  $\varepsilon \approx 0.828, 1.158$  (or at  $1/\varepsilon \approx 1.2077, 0.8636$ ) and the maximum of  $E$  occurs at  $\varepsilon \approx 1.020$  (or at  $1/\varepsilon \approx 0.980$ ).

(i.e. at  $1/\varepsilon \approx 1.357, 1.012, 0.766$ ). For the parameter values in figure 2(b), we show the corresponding  $\Delta_r$  in figure 4(a), from which we conclude that  $\Delta_r$  vanishes at  $\varepsilon \approx 0.828, 1.158$  (i.e. at  $1/\varepsilon \approx 1.208, 0.864$ ). It is worth noting that the plot of  $\Delta_r$  also has singularities which occur at exactly the same points as those in figure 2 obtained from the soliton's core.

To predict the location of the ESs, we substitute the solution of equations (12)–(14) and the root(s)  $\lambda$  of equation (18) into equations (23) to find  $E$  as a function of  $\varepsilon, c$  and  $\Lambda$ . Therefore, the existence of the ESs can be predicted by seeking for values of the parameters at which  $E = 0$ . For the parameter values used in figures 3(a) and 4(a), curves for  $E$  are displayed, respectively, in figures 3(b) and 4(b). It is seen that  $E \neq 0$  in all the figures, i.e. truly localized solitons cannot be directly predicted by the VA.

However, we can propose a conjecture, based on a ‘phenomenological’ consideration of the figures, that there are two zeros of  $\Delta_r$  on the left and right of a maximum of  $E$ . For example, in figure 3 we have the maximum of  $E$  at  $\varepsilon \approx 0.853$  (i.e. at  $1/\varepsilon \approx 1.172$ ), which is located between two adjacent numerically found zeros of  $\Delta_r$ . The same phenomenon also takes place in figure 4, where the two zero-crossing points lie between maxima of  $E$ , i.e. at  $\varepsilon \approx 1.020$  (i.e. at  $1/\varepsilon \approx 0.980$ ) in figure 4. We have also computed (not shown here) the signed measure  $\Delta_r$  and  $E$  for other combinations of parameter values, where we observed the same pattern. Thus, we conclude that, with the addition of a constant, function  $E$  may be able to predict the

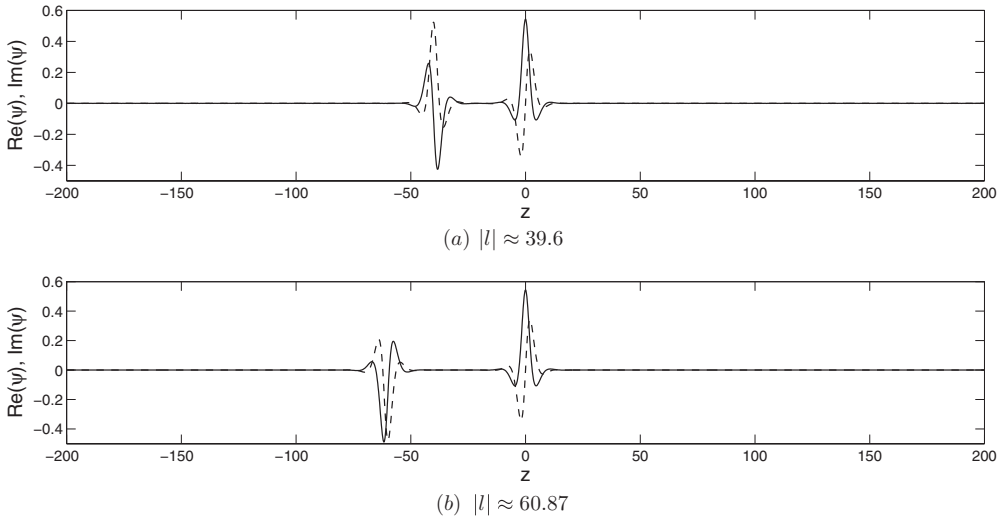


**Figure 5.** Two bound states, for  $\varepsilon = 0.7$ ,  $c = 0.7$ ,  $\Lambda = 0.7$  and  $\Delta z = 0.2$ , found numerically in the interval of  $[-200, 200]$ , for different distances between the two humps,  $|l|$ , as indicated in each panel. Solid and dashed lines depict  $\text{Re}(\psi)$  and  $\text{Im}(\psi)$ , respectively.

location of the ESs. We suspect that the missing constant, which amounts to the shift of the plot for  $E$  vertically, is related to the choice of the ansatz (see, e.g., [42] for different ansätze accounting for the oscillating tails).

### 3.3. Stability

To determine the VA-predicted stability of the soliton, we have solved the eigenvalue problem (30). For the soliton shown in figure 1(a), i.e. with  $\mathbf{x}_0 \approx [1.228, 0.554, 0.377, 0, 0, 0]^T$ , we obtain the corresponding eigenvalues  $\Omega \approx 0, 0, 0, 0, 0.436i, -0.436i$ . In addition, for the soliton in figure 1(b), i.e.  $\mathbf{x}_0 \approx [0.685, 0.414, 0.368, 0, 0, 0]^T$ , the corresponding eigenvalues are  $\Omega \approx 0, 0, 0, 0, 0.225i, -0.225i$ . As the real part of all eigenvalues is zero, we conclude that both solitons are *stable*. These results are in agreement with the numerical findings of [23].

### 3.4. Bound states

Two examples of bound states consisting of two solitons, found numerically, are presented in figure 5, each for the same parameter values.

Next, we compare the prediction presented above with the numerical results shown in figure 5. For the parameter values used in that figure, we have  $\lambda_r \approx 0.441$  and  $\lambda_i \approx 0.505$ . Note that, in terms of the above analysis, the soliton centered at  $z = 0$  in figure 5 is in fact soliton number 2. Therefore, phase difference  $\phi$  in this case is calculated as the phase of the soliton on the right minus the phase of its counterpart on the left. From the numerical results, the phase difference between the two solitons shown in the top and the bottom panels of figure 5 is given, respectively, by  $\phi \approx -2.012$  and  $\phi \approx 2.368$ , both of which correspond to  $c\lambda_i/\lambda_r > 0$ ; hence,  $n \cdot \text{sign}(\lambda_i)$  is odd. Using equation (43), we find that the best fit to the numerically computed distance in figure 5, i.e.  $|l| \approx 39.6$  and  $|l| \approx 60.87$ , is provided by

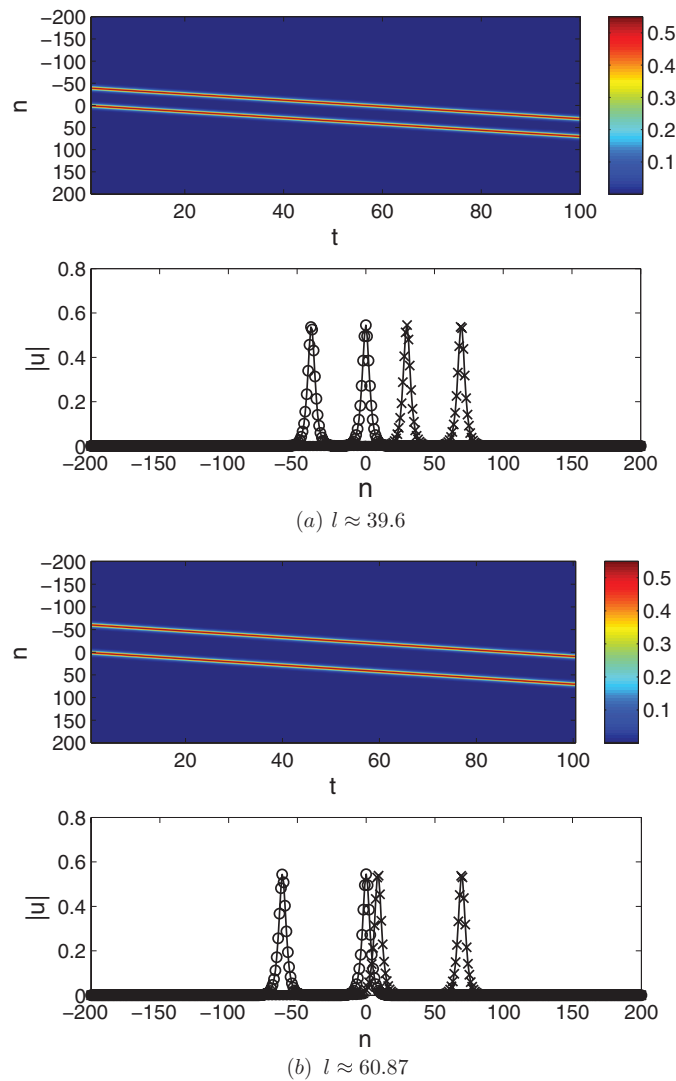


**Figure 6.** Numerical evolution of the solutions presented in figure 5, obtained by means of a numerical grid with 401 sites. Upper parts in each panel display the motion of the solution through the lattice for the first 100 time units. Shown is a spatiotemporal contour plot of the absolute value of the solution. Lower parts in each panel depict the initial (open circles) and final (crosses) profiles of the absolute value of the solution after 100 time units of the evolution.

$l_7 \approx 41.252$  and  $l_9 \approx 62.367$ . Considering the fact that equation (43) is based on a simple approximation (equations (36), (40) and (41)) and the assumption that the interacting solitons have decaying oscillating tails, the approximation is in relatively good accordance with the results provided by the numerical solution of the full equation.

Using the Runge–Kutta method, we have also carried out the numerical integration of evolution equation (1), with initial conditions taken as in figure 5. The resulting evolution of the solutions is displayed in figure 6, where we see that both solitons maintain their shapes and positions for a relatively long time.

#### 4. Conclusion

The aim of this work is to develop the semi-analytical approach to seeking traveling solitons, based on the application of the VA to the differential–difference form of the DNLSE with saturable nonlinearity, in the moving coordinate frame. The predicted shapes of the solitons are in good agreement with the numerical findings. The VA is also extended to examine the stability of the traveling solitons, showing that they are stable, which is consistent with the previous work [23]. Furthermore, the VA was developed to predict the locations of the exceptional solutions for genuine traveling solitons with strictly vanishing tails. Bound states of two solitons were briefly considered too. In the latter case, the VA predicts the distance between two solitons forming the bound state. In the numerical part of the work, we have made use of the numerical scheme for the DNLSE written in the moving coordinate frame, which is an equation of the differential–difference type. Using the Newton–Raphson method, we have confirmed the existence of exceptional solutions for traveling discrete solitons (which are ‘embedded solitons’, in this sense), earlier predicted by means of a different numerical algorithm. We have compared the analytical results based on the VA and the numerical findings, concluding that they are in good agreement.

#### Acknowledgments

MS acknowledges the Ministry of National Education of the Republic of Indonesia for financial support.

#### References

- [1] Peierls R 1940 The size of a dislocation *Proc. Phys. Soc. Lond.* **52** 34  
Nabarro F R N 1947 Dislocations in a simple cubic lattice *Proc. Phys. Soc. Lond.* **59** 256
- [2] Kevrekidis P G (ed) 2009 *Discrete Nonlinear Schrödinger Equation: Mathematical Analysis, Numerical Computations and Physical Perspectives* (New York: Springer)
- [3] Lederer F, Stegeman G I, Christodoulides D N, Assanto G, Segev M and Silberberg Y 2008 Discrete solitons in optics *Phys. Rep.* **463** 1–126  
Kartashov Y V, Vysloukh V A and Torner L 2009 Soliton shape and mobility control in optical lattices *Prog. Opt.* **52** 63
- [4] Smerzi A and Trombettoni A 2003 Nonlinear tight-binding approximation for Bose–Einstein condensates in a lattice *Phys. Rev. A* **68** 023613  
Carretero-González R, Frantzeskakis D J and Kevrekidis P G 2008 Nonlinear waves in Bose–Einstein condensates: physical relevance and mathematical techniques *Nonlinearity* **21** R139
- [5] Eilbeck J C 1986 Numerical simulations of the dynamics of polypeptide chains and proteins *Computer Analysis for Life Science: Progress and Challenges in Biological and Synthetic Polymer Research* ed C Kawabata and A R Bishop (Tokyo: Ohmsha) pp 12–21
- [6] Feddersen H 1991 Solitary wave solutions to the discrete nonlinear Schrödinger equation *Nonlinear Coherent Structures in Physics and Biology (Lecture Notes in Physics vol 393)* ed M Remoissenet and M Peyrard (Berlin: Springer) pp 159–67
- [7] Duncan D B, Eilbeck J C, Feddersen H and Wattis J A D 1993 Solitons on lattices *Physica D* **68** 1–11
- [8] Gómez-Gardeñes J, Falo F and Floría L M 2004 Mobile localization in nonlinear Schrödinger lattices *Phys. Lett. A* **332** 213  
Gómez-Gardeñes J, Floría L M, Peyrard M and Bishop A R 2004 Nonintegrable Schrödinger discrete breathers *Chaos* **14** 1130
- [9] Pelinovsky D E, Melvin T R O and Champneys A R 2007 One-parameter localized traveling waves in nonlinear Schrödinger lattices *Physica D* **236** 22–43
- [10] Melvin T R O, Champneys A R and Pelinovsky D E 2009 Discrete traveling solitons in the Salerno model *SIAM J. Appl. Dyn. Syst.* **8** 689–709

- [11] Fleischer J W, Segev M, Efremidis N K and Christodoulides D N 2003 Observation of two-dimensional discrete solitons in optically induced nonlinear photonic lattices *Nature* **422** 147
- [12] Neshev D, Alexander T J, Ostrovskaya E A, Kivshar Y S, Martin H, Makasyuk I and Chen Z 2004 Observation of discrete vortex solitons in optically induced photonic lattices *Phys. Rev. Lett.* **92** 123903  
Fleischer J W, Bartal G, Cohen O, Manela O, Segev M, Hudock J and Christodoulides D N 2004 Observation of vortex-ring ‘discrete’ solitons in 2D photonic lattices *Phys. Rev. Lett.* **92** 123904
- [13] Yang J, Makasyuk I, Kevrekidis P G, Martin H, Malomed B A, Frantzeskakis D J and Chen Z G 2005 Necklace-like solitons in optically induced photonic lattices *Phys. Rev. Lett.* **94** 113902
- [14] Wang X S, Chen Z G and Kevrekidis P G 2006 Observation of discrete solitons and soliton rotation in optically induced periodic ring lattices *Phys. Rev. Lett.* **96** 083904
- [15] Kevrekidis P G, Chen Z G, Malomed B A, Frantzeskakis D J and Weinstein M I 2005 Spontaneous symmetry breaking in photonic lattices: theory and experiment *Phys. Lett. A* **340** 275–80
- [16] Sakaguchi H and Malomed B A 2005 Higher-order vortex solitons, multipoles and supervortices on a square optical lattice *Europhys. Lett.* **72** 698–704  
Kevrekidis P G, Susanto H and Chen Z 2006 High-order-mode soliton structures in two-dimensional lattices with defocusing nonlinearity *Phys. Rev. E* **74** 066606
- [17] Carretero-González R, Talley J D, Chong C and Malomed B A 2006 Multistable solitons in the cubic–quintic discrete nonlinear Schrödinger equation *Physica D* **216** 77–89  
Chong C, Carretero-González R, Malomed B A and Kevrekidis P G 2009 Multistable solitons in higher-dimensional cubic–quintic nonlinear Schrödinger lattices *Physica D* **238** 126–36
- [18] Vicencio R A and Johansson M 2006 Discrete soliton mobility in two-dimensional waveguide arrays with saturable nonlinearity *Phys. Rev. E* **73** 046602
- [19] Hadžievski L, Maluckov A, Stepić M and Kip D 2004 Power controlled soliton stability and steering in lattices with saturable nonlinearity *Phys. Rev. Lett.* **93** 033901
- [20] Khare A, Rasmussen K Ø, Samuelsen M R and Saxena A 2005 *J. Phys. A: Math. Gen.* **38** 807
- [21] Khare A, Rasmussen K Ø, Samuelsen M R and Saxena A 2009 *J. Phys. A: Math. Theor.* **42** 085002
- [22] Melvin T R O, Champneys A R, Kevrekidis P G and Cuevas J 2006 Radiationless travelling waves in saturable nonlinear Schrödinger lattices *Phys. Rev. Lett.* **97** 124101
- [23] Melvin T R O, Champneys A R, Kevrekidis P G and Cuevas J 2008 Travelling solitary waves in the discrete Schrödinger equation with saturable nonlinearity: existence, stability and dynamics *Physica D* **237** 551–67
- [24] Yang J, Malomed B A and Kaup D J 1999 Embedded solitons in second-harmonic-generating systems *Phys. Rev. Lett.* **83** 1958–61  
Champneys A R, Malomed B A, Yang J and Kaup D J 2001 ‘Embedded solitons’: solitary waves in resonance with the linear spectrum *Physica D* **152–153** 340–54
- [25] Champneys A R and Malomed B A 1999 Moving embedded solitons *J. Phys. A: Math. Gen.* **32** L547–53
- [26] Gonzalez-Perez-Sandi S, Fujioka J and Malomed B A 2004 Embedded solitons in dynamical lattices *Physica D* **197** 86–100  
Yagasaki K, Champneys A R and Malomed B A 2005 Discrete embedded solitons *Nonlinearity* **18** 2591–613  
Malomed B A, Fujioka J, Espinosa-Ceron A, Rodriguez R F and Gonzalez S 2006 Moving embedded lattice solitons *Chaos* **16** 013112
- [27] Oxtoby O F and Barashenkov I V 2007 Moving solitons in the discrete nonlinear Schrödinger equation *Phys. Rev. E* **76** 036603
- [28] Malomed B A and Weinstein M I 1996 Soliton dynamics in the discrete nonlinear Schrödinger equation *Phys. Lett. A* **220** 91–6
- [29] Kaup D J 2005 Variational solutions for the discrete nonlinear Schrödinger equation *Math. Comput. Simul.* **69** 322–33
- [30] Chong C and Pelinovsky D E 2011 Variational approximations of bifurcations of asymmetric solitons in cubic–quintic nonlinear Schrödinger lattices *Discrete Control Dyn. Syst. S* **4** 1019–32
- [31] Chong C, Pelinovsky D E and Schneider G 2011 On the validity of the variational approximation in discrete nonlinear Schrödinger equations *Physica D* **241** 115–24
- [32] Kaup D J and Malomed B A 2003 Embedded solitons in Lagrangian and semi-Lagrangian systems *Physica D* **184** 153–61
- [33] Gradshteyn I S and Ryzhik I M 2000 *Tables of Integrals, Series and Products* (New York: Academic)
- [34] Flytzanis N, Malomed B A and Wattis J A D 1993 Analysis of stability of solitons in one-dimensional lattices *Phys. Lett. A* **180** 107–12
- [35] Kivshar Y S, Champneys A R, Cai D and Bishop A R 1998 Multiple states of intrinsic localized modes *Phys. Rev. B* **58** 5423–8

- [36] Kapitula T, Kevrekidis P G and Malomed B A 2001 Stability of multiple pulses in discrete systems *Phys. Rev. E* **63** 036604
- [37] Kevrekidis P G 2001 Multipulses in discrete Hamiltonian nonlinear systems *Phys. Rev. E* **64** 026611
- [38] Malomed B A and Nepomnyashchy A A 1994 Stability limits for arrays of kinks in two-component nonlinear systems *Europhys. Lett.* **27** 649
- [39] Malomed B A 1998 Potential of interaction between two- and three-dimensional solitons *Phys. Rev. E* **58** 7928
- [40] Weideman J and Reddy S 2000 A MATLAB differentiation matrix suite *ACM Trans. Math. Softw.* **26** 465–519
- [41] Trefethen L N 2000 *Spectral Methods in MATLAB* (Philadelphia, PA: SIAM)
- [42] Boyd J P 1998 *Weakly Nonlocal Solitary Waves and Beyond-all-orders Asymptotics* (Dordrecht: Kluwer)